International Journal of Minerals, Metallurgy and Materials
Volume 28, Number 10, October 2021, Page 1726
https://doi.org/10.1007/s12613-020-2146-5

Electrical, thermal and electrochemical properties of γ-ray-reduced graphene oxide

M.M. Atta[1)], *H.A. Ashry*[1)], *G.M. Nasr*[2)], *and H.A. Abd El-Rehim*[3)]

1) Radiation Physics Department, National Center for Radiation Research and Technology (NCRRT), Atomic Energy Authority, Cairo 11787, Egypt
2) Physics Department, Faculty of Science, Cairo University, Cairo 12613, Egypt
3) Radiation Chemistry Department, National Center for Radiation Research and Technology (NCRRT), Atomic Energy Authority, Cairo 11787, Egypt
(Received: 5 March 2020; revised: 9 July 2020; accepted: 15 July 2020)

Abstract: The properties of γ-ray-reduced graphene oxide samples (GRGOs) were compared with those of hydrazine hydrate-reduced graphene oxide (HRGO). Fourier transform infrared spectroscopy, X-ray diffractometry, Raman spectroscopy, Brunauer–Emmett–Teller surface area analysis, thermogravimetric analysis, electrometry, and cyclic voltammetry were carried out to verify the reduction process, structural changes, and defects of the samples, as well as to measure their thermal, electrical, and electrochemical properties. Irradiation with γ-rays distorted the structure of GRGOs and generated massive defects through the extensive formation of new smaller sp^2-hybridized domains compared with those of HRGO. The thermal stability of GRGOs was higher than that of HRGO, indicating the highly efficient removal of thermally-labile oxygen species by γ-rays. RRGO prepared at 80 kGy showed a pseudocapacitive behavior comparable with the electrical double-layer capacitance behavior of HRGO. Interestingly, the specific capacitance of GRGO was enhanced by nearly three times compared with that of HRGO. These results reflect the advantages of radiation reduction in energy storage applications.

Keywords: graphene; γ-ray; electrical; thermal; electrochemical

1. Introduction

The unique physical properties of graphene render it an interesting material for many research fields, especially in energy storage applications, such as supercapacitors [1], Li-ion batteries [2], and solar cells [3]. Graphene may be prepared from a number of synthetic methods, including epitaxial growth [4], chemical vapor deposition [5], and mechanical exfoliation [6]. Graphite oxide (GO) reduction is a common method used for the scalable production of graphene; however, the product obtained is often of low quality [7]. The reduction of GO may be carried out through thermal means, during which water and oxygen functional groups are eliminated by high temperature [7–8], or by using chemical agents such as hydrazine, hydroiodic, and hydrobromic [8–9]. Natural products, such as vitamins, amino acids, and *Lycium barbarum* extract, have also been used for GO reduction [10–11]. Different types of radiation (e.g., ionizing and non-ionizing) from UV light [8], microwaves [12], laser [13], plasma [14], and X-rays [15] were employed to achieve GO reduction. In 2012, Zhang *et al*. [16] used γ-rays to reduce GO in a water/alcohol system for the first time. The total absorbed dose was 35.3 kGy and the dose rate was 0.88 $kGy \cdot h^{-1}$. Compared to chemical and thermal reduction, radiation reduction is more environment-friendly, non-toxic, temperature-independent, and inexpensive [17].

The reduction of GO by γ-rays is based on the radiolysis of water to create reductive (H) and oxidative (OH) radical species. Addition of alcohol is necessary to complete the reduction process; in this case, the alcohol suppresses oxidative radicals from further GO oxidation. Oxygen-free (deoxygenation) has been reported to be crucial for the radiation reduction of GO in alcohol/water systems [16]; thus, this technique has been used by many researchers to synthesize graphene and graphene-based materials. For example, three dimensional (3D) graphene aerogels with porous honeycomb-like structures could be prepared by applying an absorbed dose 200 kGy and nitrogen bubbling deoxygenation for 10 min [18]. Reduced graphene oxide (RGO)–Ni nanocomposites with enhanced electromagnetic absorption ability could be successfully prepared by γ-ray irradiation [19]. A 3D graphene–Pt nanoparticle-based aerogel composite has

Corresponding author: M.M. Atta E-mail: mmatta2007@yahoo.com; mohatta2014@gmail.com

been synthesized by γ-ray irradiation in an ethanol/water system under N_2 protection [20]. Similarly, TiO_2-decorated RGO has been synthesized by using γ-ray irradiation for 16 h at a dose rate of 5 kGy·h^{-1} [21]. Composites of RGO/carbon nanotubes have been prepared via γ-rays by applying an absorbed dose of 30–200 kGy and deoxygenation by Ar bubbling for 30 min [22]. Composites of RGO/ organic inhibitor have offered high corrosion protection efficiency for AISI 316 in 0.5 M sulfuric acid solutions [23]. Composites of different noble metal (e.g., Ag, Au, and Pt) nanoparticles and GO have been successfully prepared via γ-ray irradiation without a scavenger. Here, aqueous solutions of $AgNO_3$, $HAuCl_4{\cdot}4H_2O$, and $H_2PtCl_6{\cdot}6H_2O$ were added to GO solution, and the mixtures were purged with Ar for 30 min and irradiated by a ^{60}Co γ-ray irradiation source with a dose rate of 2.7 kGy·h^{-1} and absorbed dose of 150 kGy [24].

GO has been successfully reduced in *N*,*N*-dimethylformamide (DMF) by using high absorbed doses of γ-rays [17,25]. The same concept has been applied to reduce GO through electron beam irradiation, instead of γ-ray irradiation. For instance, RGO could be successfully obtained by electron beam irradiation of a GO suspension/isopropanol solution placed in a sealed bag filled with N_2 gas [26]. The reduction degree of RGO could be controlled by varying the electron beam dose from 0 to 40 kGy. In another report [27], GO in a water/ethanol system purged with N_2 gas was reduced by electron beam absorbed doses ranging from 50 to 200 kGy. N_2-doped graphene could be obtained by irradiating a GO aqueous solution containing isopropyl alcohol and aqueous NH_3 with electron beams with absorbed doses of 100, 200, and 300 kGy [28].

The physical properties and quality of graphene are affected by its synthesis method and, in turn, influence the quality and efficiency of their resulting applications. Thus, in this work, we compare the structural, electrical, thermal, and electrochemical properties of hydrazine-reduced graphene oxide (HRGO) with those of γ-ray-reduced graphene oxide (GRGO) prepared at different absorbed doses. Compared with previous studies [16], the GRGOs in the present work were obtained at a relatively higher dose rate of 2 kGy·h^{-1} and without deoxygenation. We found that radiation reduction is an ideal method for RGO preparation, especially when the resulting RGO is to be applied in devices such as supercapacitors and thermal resistors.

2. Experimental

2.1. Materials

Fine graphite powder (<50 μm) was purchased from Merk (Germany). H_2SO_4 (98%), H_3PO_4 (85%), polytetrafluoroethylene, carbon black, and hydrazine hydrate were purchased from Sigma–Aldrich (USA). $KMnO_4$, H_2O_2 (35%), DMF, ethanol (96%), and HCl were purchased from El Nasr Pharmaceutical Chemicals Company (Egypt).

2.2. Sample preparation

(1) Graphite oxide preparation.

GO was synthesized from graphite according to an improved Hummer's method [29]. This method yields GO with a more oxidized and regular structure compared with those obtained from the original and other modified Hummer's methods [29].

(2) γ-ray-reduced graphene oxide preparation.

Exactly 100 mg of GO was exfoliated in 50 mL of distilled water by a sonication probe for approximately 30 min. After exfoliation, 50 mL of ethanol was added to the above mixture, which was subsequently irradiated by γ-rays from a ^{60}Co source at the National Center for Radiation Research and Technology–Egyptian Atomic Energy Authority. Total absorbed doses of 20, 40, and 80 kGy and a dose rate of 2 kGy·h^{-1} were used to obtain three different samples. The obtained mixtures were precipitated, washed with distilled water, and dried at 60°C in a vacuum oven for approximately12 h.

(3) Hydrazine-reduced graphene oxide preparation.

Exactly 300 mg of GO was exfoliated in 100 mL of distilled water by a sonication probe for approximately 30 min. Next, 0.3 mL of hydrazine hydrate was added to the GO solution, which was subsequently heated in an oil bath at 80°C with continuous stirring for approximately 24 h. Finally, the obtained mixture was precipitated, washed with distilled water, and dried at 60°C in a vacuum oven.

2.3. Characterization

Structural explorations were carried out by X-ray diffractometry (XRD, Shimadzu) with Cu K_α radiation (λ = 0.15405 nm) at 2θ of 4°–90°. The generator voltage was 40 kV, and the generator current was 30 mA. All measurements were carried out in continuous scan mode, the scan speed was 8°·min^{-1}, and the sampling pitch was 0.02°. The chemical structure of the samples was investigated using Fourier transform infrared spectroscopy (FTIR; Prestige-21; Shimadzu). The FT-IR spectra were recorded using KBr as the mulling agent in the region of 400–4000 cm^{-1}. A Witec Alpha 300 R confocal Raman spectroscope with a Nd : Yag laser excitation source (532 nm) was employed to evaluate the structural defects of the samples in the range of 400–2500 cm^{-1} at room temperature. The bulk electrical conductivity of the samples was measured using the two-probe method at room temperature. Here, dry powdered samples were pressed into pellets of ~1 mm thickness and ~10 mm diameter using a stainless steel die in a hydraulic press at 300 MPa. A Keithley 2400 instrument was used as a DC power source, and a Keithley 6517 instrument was used as an electrometer. The surface area of the samples was determined from N_2 adsorption–desorption isotherms obtained from a NOVA 4200e Series surface area and pore size analyzer at liquid N_2 temperature. Pri-

or to the measurements, samples of approximately 200 mg were degassed under vacuum at 350°C for 24 h. The thermal stability of the samples was tested via thermogravimetric analysis (TGA; Shimadzu 50). The samples were heated at a rate of 10°C·min^{-1} in the temperature range of 25–700°C under a N_2 atmosphere. An SP-300 potentiostat (Bio-Logic) was used to investigate the electrochemical properties of the GRGOs and HRGO. The electrochemical cell consisted of a glassy carbon electrode (3 mm diameter) modified with GRGO or HRGO powders as the working electrode, a graphite rod as the counter electrode, and a KCl electrode as the reference electrode. The working electrode was fabricated by dispersing 1 mg of each GRGO or HRGO sample in 1 mL of DMF under sonication for approximately 2 h. Exactly 50 μL of each solution was then drop-cast on a pre-cleaned GC, which was subsequently dried under a vacuum at 50°C.

3. Results and discussion

3.1. X-ray diffraction analysis

XRD provides essential information on the structural changes occurring in GO during reduction. Fig. 1 presents the XRD patterns of graphite, GO, HRGO, and the GRGO powders. The XRD pattern of graphite shows a sharp diffraction peak at 26.32°, which corresponds to a *d*-spacing of 0.338 nm and reflects a tightly packed monolayer of carbon atoms. The XRD pattern of GO shows a sharp peak at 8.5° with a *d*-spacing of 1.036 nm; this peak corresponds to the (002) plane and reflects the presence of rich oxygen functional groups held between graphitic layers during the oxidation process [30]. The XRD pattern of GRGO prepared at 20 kGy shows the splitting of the (002) peak into three major

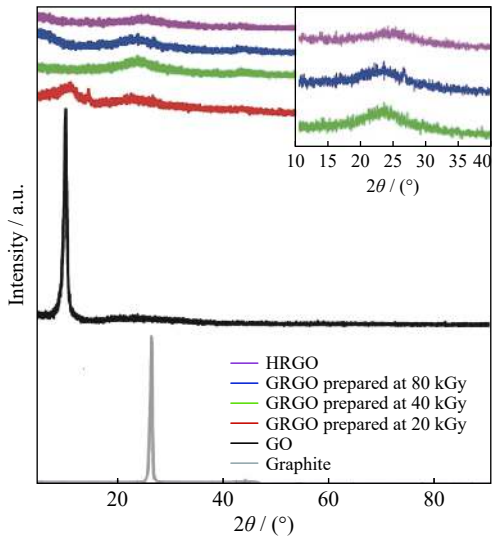

Fig. 1. XRD pattern of graphite, graphene oxide (GO), hydrazine hydrate reduced graphene oxide (HRGO), and γ-rays-reduced graphene oxide samples (GRGOs) prepared at different absorbed doses.

broad peaks: the first one is located at 10.6° with a *d*-spacing of 0.83 nm, the second one is located at 13.9° with a *d*-spacing of 0.635 nm, and the third one is located at 22.7° with a *d*-spacing of 0.39 nm. The existence of these peaks with reduced interlayer spacing values compared with that of GO is ascribed to the partial elimination of oxidized species in GO during irradiation [16]. In other words, GO is partially reduced by irradiation at 20 kGy.

The XRD pattern of GRGO prepared at 40 kGy, which is shown in the inset of Fig.1, reveals a broad peak at 23° with a *d*-spacing of 0.368 nm; this result confirms the removal most of the oxygen functional groups and successful reduction of GO [16]. The XRD pattern of the GRGO sample prepared at an irradiation dose of 80 kGy is similar to that of the sample prepared at 40 kGy but presents lower intensities and a slight shift of the main peak at 23° to 23.1°, thereby indicating a slight decrease in *d*-spacing to 0.383 nm. In addition, a small peak develops at 26.34° (*d*-spacing, 0.0338 nm). This result indicates that the sample prepared at 80 kGy has a higher reduction degree than the sample prepared at 40 kGy. Similarly, the broad peak of HRGO at $2\theta = 23.7°$ with low intensity and *d*-spacing of 0.370 nm reveal that this sample has a higher reduction degree compared with the GRGOs prepared at 40 and 80 kGy [31].

3.2. Fourier transform infrared spectroscopic analysis

FTIR provides essential information on the oxygen functional groups of GO and could help verify the different reduction processes in our samples.

Fig. 2 shows the FTIR spectra of GO, HRGO, and GRGOs prepared at different doses. GO shows a strong and broadband at approximately 3350 cm^{-1}, which is attributed to the O–H stretching vibrations of water and C–OH groups. Strong bands at 1735 and 1620 cm^{-1} respectively correspond to the stretching vibrations of carbonyl (C=O) groups and the skeletal vibrations of unoxidized graphitic domains (C=C) [32]. Epoxide (C–O) stretching vibrations are evidenced by peaks at approximately 1210 and 1030 cm^{-1}. The band located at ~1400 cm^{-1} corresponds to the carboxyl (C–OH) group [33]. These bands reflect the abundance of water and oxygen functional groups in graphite during the oxidation process and are consistent with XRD data. The intensity of most of the GO bands in the spectrum of GRGO prepared at 20 kGy weakened or decreased, especially those at 3350, 1735, and 1030 cm^{-1}. The decreased intensity of these oxygen-containing groups reflects the deoxygenation of GO during γ-ray irradiation [34]. The band located at 1200 cm^{-1} is the only peak that exhibits increased intensity after irradiation, which is attributed to the reconstruction of some oxygen functional groups. The band at 2950–2850 cm^{-1} is attributed to stretching vibrations of C–H groups, thereby indicating that some alkyl groups could attach to the graphene sheets under γ-ray irradiation [25]. The residual intensities of

the bands of oxygen-containing functionalities indicate that the GRGO sample prepared at 20 kGy retains oxygen species; in other words, the sample is only partially reduced. This result is consistent with the XRD data. The elimination of GO bands from the spectra of GRGOs prepared at 40 and 80 kGy and HRGO reflects the removal of residual oxygen functional groups and efficient reduction of GO by γ-ray irradiation and hydrazine [34]. The red-shifting of the C=C band to ~1560 cm^{-1} indicates the reconstruction of aromatic skeletons [25].

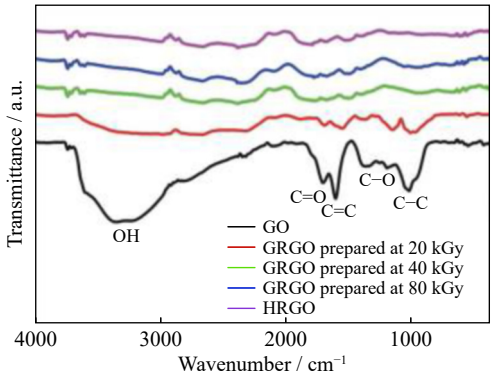

Fig. 2. FTIR spectra of GO, HRGO, and GRGOs prepared at different absorbed doses.

3.3. Raman spectroscopic analysis

Raman spectroscopy, a non-destructive tool widely used to study carbon-related materials, was employed in the present research to confirm the reduction of the samples and assess structural changes in graphite and GO during oxidation and reduction. The Raman spectra of graphite, GO, GRGOs, and HRGO are presented in Fig. 3. The spectra of the bulk graphite display two strong bands at ~1578 and ~1350 cm^{-1}. The first peak is called the G band corresponds to a doubly degenerate E_{2g} mode at the zone center. The second peak is called the D band and generally Raman inactive for pristine graphene; the detection of this peak indicates broken symmetry at edges or defective samples [35–36]. The D and G bands of GO, GRGOs, and HRGO show changes similar to those observed in the transition of graphite to amorphous carbon [37]. Higher disorder in graphite has been reported lead to the broadening of G and D bands and increased D band intensity [37]. This finding and our observation of narrower D and G bands in the Raman spectra of the GRGOs reveal that our samples have a more regular structure than HRGO [31]. The shortening and broadening of the G and D bands of GO, GRGOs, and HRGO with increasing D band intensity indicates the higher defect level of these samples compared with that of graphite. The G band position of GO, GRGOs, and HRGO is ~2–8 cm^{-1} higher than that of bulk graphite because of chemical doping [35]. The red-shifting of the D band to ~1340 cm^{-1} confirms the successful reduction of the GRGO and HRGO samples [22]. Changes in the D and G band intensities of GO under different reduction conditions reveal changes in the degree of conjugation and functionalization in the obtained GRGOs and HRGO [31]. The ratio of the intensities of the D and G bands (I_D/I_G) of the graphitic materials is often used as an indicator of their degree of structural defects and disorders or graphitic quality. According to the Tuinstra–Koenig relation [38], I_D/I_G increases with increasing disorder at a fixed wavelength. The I_D/I_G of graphite increased from 0.38 to 1.02 in GO because of the presence of oxygen groups on the basal planes or edges of graphene sheets [39]. As shown in Fig. 4, the I_D/I_G ratios of the GRGOs and HRGO are consistently higher than that of GO due to the decrease in average size of sp^2 domains upon reduction of GO [40]. These results confirm the restoration of the sp^2-hybridized carbon network of GO through γ-ray irradiation and chemical reduction [41].

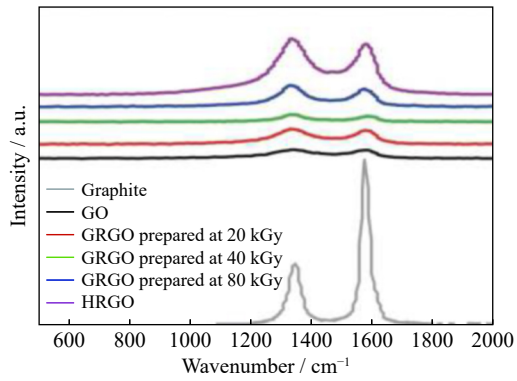

Fig. 3. Raman spectra of graphite, GO, HRGO, and GRGOs prepared at different absorbed doses.

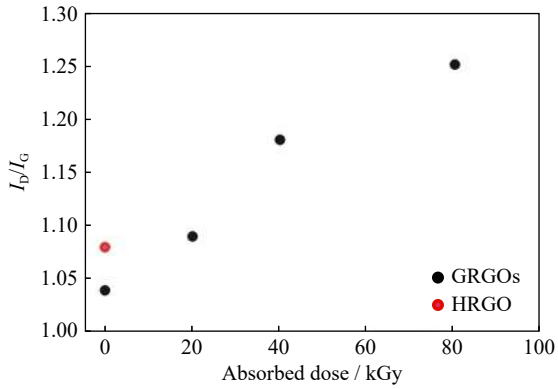

Fig. 4. I_D/I_G ratios of GO (0 kGy), GRGOs, and HRGO.

The I_D/I_G ratio generally increased with increasing absorbed dose, which means radiation reduction alters the GO structure to generate massive defects. Such behavior indicates that the reduction degree (or the recovery of sp^2 domains) of GRGOs increases with increasing radiation absorbed dose. This result is consistent with the XRD findings. The higher I_D/I_G ratios of GRGOs compared with that of

HRGO may be explained by the extensive formation of new smaller sp^2-hybridized domains by γ-ray irradiation in the latter [42].

3.4. Thermogravimetric analysis

TGA is an effective tool to study the thermal stability of different samples and confirm the occurrence of reduction. Fig. 5 shows the TGA curves of GO, HRGO, and GRGOs prepared at different absorbed doses. The TGA curve of GO shows four distinct weight-loss segments. The first occurs from ambient temperature to ~150°C (20%) and is attributed to the loss of loosely bound or adsorbed water and gas molecules. The second weight loss segment occurs at 150–260°C (~23%) and is caused by the decomposition of labile oxygen groups, such as carboxylic, anhydride, or lactone groups. The third weight loss segment occurs at 250–560°C (~20%) and is attributed to the presence of more thermally-stable oxygen functionalities. Finally, the fourth weight-loss segment occurs at 600–700°C and is due to the bulk pyrolysis of the carbon skeleton [43]. The TGA curves of the GRGOs reveal more gradual weight losses in the first three segments with increasing irradiation dose, which indicates that the reduction degree of these samples increases with increasing γ-ray dose. Moreover, the RRGOs prepared at 40 and 80 kGy are more thermally-stable than CRGO at these temperature ranges, thereby indicating more effective removal of thermally-labile oxygen species by γ-ray irradiation reduction compared with chemical reduction [41,44]; this result is highly similar to previous reports [45]. The higher residual weight of HRGO compared with those of the GRGO samples at temperatures above 560°C indicates its higher reduction degree. Taken together, the TGA results are consistent with the XRD and Raman results.

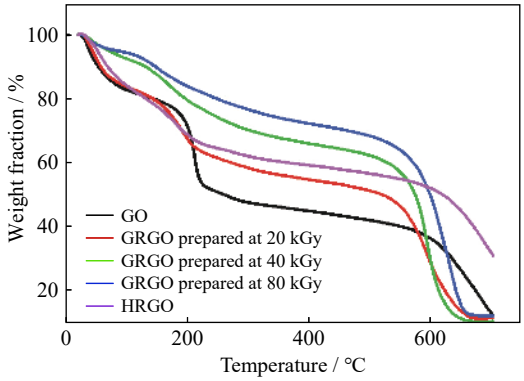

Fig. 5. TGA curves of GO, HRGO, and GRGO samples prepared at different absorbed doses.

3.5. Electrical conductivity

Fig. 6 shows the current–voltage (*I–V*) characteristics curves of graphite, GO, HRGO, and GRGO powders with the corresponding fitting lines. The graphite shows a strong linear *I–V* dependency. A drastic drop in *I* of GO indicated its insulating nature compared with the graphite, and the current restored greatly in GRGOs and HRGO approaching to that of the pristine graphite. Fig. 7 illustrates the calculated 3D bulk electrical conductivities (σ) of the GRGO powders in comparison with that of HRGO.

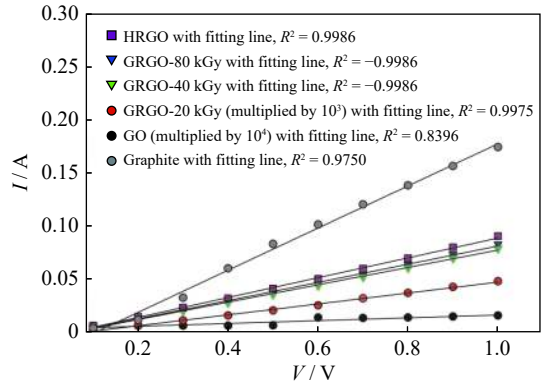

Fig. 6. *I–V* characteristics of graphite, GO, HRGO, and GRGOs prepared at different irradiation doses.

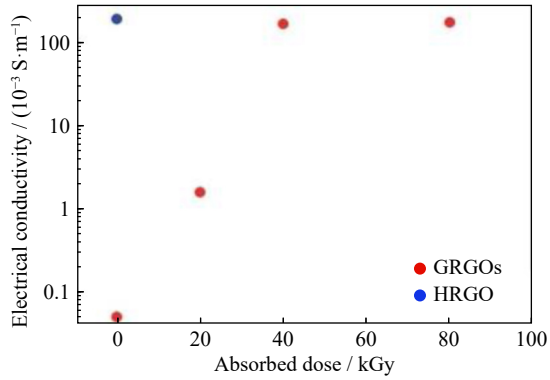

Fig. 7. Electrical conductivities of GO (0 kGy), GRGOs, and HRGO.

The poor conductivity of GO (5.04×10^{-5} S·m^{-1}) compared with that of graphite (~0.97 S·m^{-1}) is strongly correlated with the presence of sp^3-hybridized carbons, which represent transport barriers and lead to the absence or disturbance of percolating pathways among sp^2 carbon clusters, in the sample. The electrical conductivity of the GRGO powders improved with the γ-ray dose. The increased conductivity of GRGOs compared with that of GO may be attributed to the restoration of conjugated sp^2-hybridized carbons during the reduction process; moreover, the observed increase in conductivity with increasing irradiation dose is consistent with previous results [46]. The electrical conductivity of GRGO prepared at 80 kGy (0.170 S·m^{-1}) is higher than that prepared at 40 kGy (0.160 S·m^{-1}) because of differences in their reduction degrees, as described earlier. The higher conductivity of HRGO (0.192 S·m^{-1}) compared with that of GRGO may be attributed to the lower *d*-spacing of the

former, as confirmed previously by XRD, and the high defect level of the GRGOs, as deduced from the Raman spectra. Defects act as scattering sites and limit charge transport by limiting the electron mean free path and decreasing conductivity [47]. High defect ratios of the GRGO and HRGO powders lead to lower conductivities compared with that of pristine graphite, which is consistent with previous studies [48–51]

3.6. Brunauer–Emmett–Teller surface area analysis

Brunauer–Emmett–Teller (BET) surface area analysis was conducted to estimate the specific surface areas of HRGO and GRGO prepared at 80 kGy.

Fig. 8 shows the typical N_2 adsorption–desorption isotherms of GRGO and HRGO samples. The adsorption curves clearly show type-IV isotherms, thus confirming the mesoporous nature of both samples. The BET specific surface areas of GRGO and HRGO were calculated to be 382.2 and 306.3 $m^2 \cdot g^{-1}$, respectively. The larger surface area of GRGO in comparison with that of HRGO may be attributed to the use of irradiation reduction as a mild method that restrains the aggregation of GRGO with more regular structure sheets than HRGO as confirmed by Raman results [22]. The BET surface areas of GRGO and HRGO are lower than the theoretical limit of graphene (2630 $m^2 \cdot g^{-1}$). This finding indicates that both samples are incompletely exfoliated and retain some stacked graphitic layers [52–53].

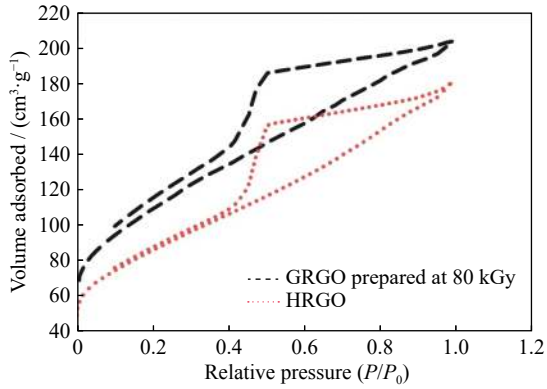

Fig. 8. N_2 adsorption and desorption isotherms of HRGO and GRGO prepared at 80 kGy.

The pore size distribution curves of GRGO and HRGO are derived from the corresponding desorption branches via the Barret–Joyner–Halenda method and shown in Fig. 9. The samples show similar pore size distributions and mesopores. The predominant pore diameter of GRGO, at 3.71 nm, is similar to that of HRGO (3.70 nm).

3.7. Comparison of the electrochemical behaviors of GRGO and HRGO

Because of its low cost, wet-chemical properties, scalable

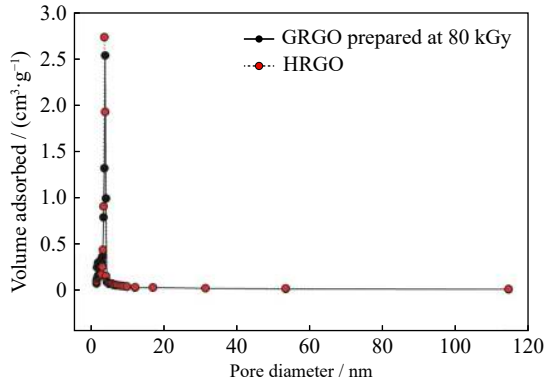

Fig. 9. Pore size distributions of HRGO and GRGO prepared at 80 kGy.

production, and high-density active defect sites, RGO is commonly used as an active material in conventional supercapacitors and micro-supercapacitor construction [54]. In this section, the electrochemical behaviors of GRGO and HRGO are compared to assess their performance as supercapacitor materials.

According to the FTIR, XRD, and TGA results, among GRGOs samples, that obtained at 80 kGy has the highest reduction degree and thermal stability; thus, this sample was selected for further electrochemical studies in comparison with HRGO. The electrochemical performances and capacitive behaviors of HRGO and GRGO prepared at 80 kGy were analyzed using cyclic voltammetry (CV) in 1 mol of KOH over the potential range of 0.6–1.4 V versus Ag/AgCl.

Figs. 10 and 11 respectively show the CV curves of HRGO and GRGO at different scan rates of 100–500 $mV \cdot s^{-1}$. The CV curves of HRGO exhibit approximately the same rectangular shape at various scan rates, indicating a characteristic electrical double-layer capacitance (EDLC) behavior. By contrast, the CV curves of GRGO show deviations from a rectangular shape, indicating pseudocapacitive characteristics. This behavior may be attributed to the higher ratio of residual oxygen groups (i.e., lower reduction degree) in GRGO compared with that in HRGO, as deduced from the XRD and TGA results [55]. Besides improving the surface efficiency of

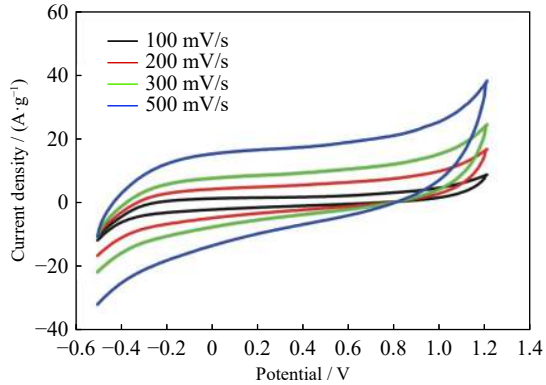

Fig. 10. CV curves of HRGO sample at different scan rates.

graphene during electrochemical cycling, oxygen functional groups also confer the material with a high pseudocapacitance [55–56].

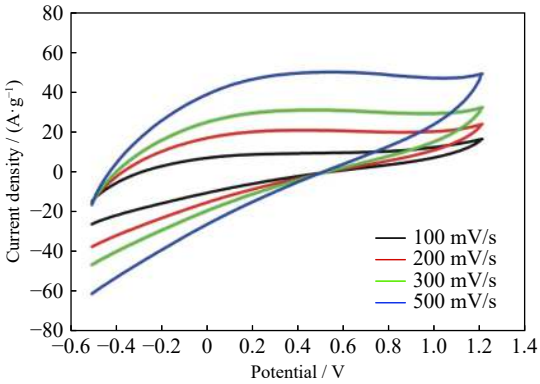

Fig. 11. CV curves of GRGO sample prepared at 80 kGy at different scan rates.

The specific capacitance of the two electrodes was calculated from the CV curves according to the general equation described in a previous report [57].

Plots of the calculated specific capacitance versus scan rate of GRGO and HRGO are provided in Fig. 12. The specific capacitance of GRGO is nearly three times higher than that of HRGO. The capacitance performance of carbon materials is strongly dependent on their specific surface area and pore size [58]. The structural defects and surface chemistry (i.e., nature and amount of oxygen groups) of carbon materials are known to improve their capacitive performance. Defects, heteroatom doping, and residual oxygen vary the electro-neutrality of graphene and allow ions and electrolytes facile access to the electrode, thereby resulting in increased pseudocapacitance, high charge storage capacity, and fast charge–discharge rates [59–64].

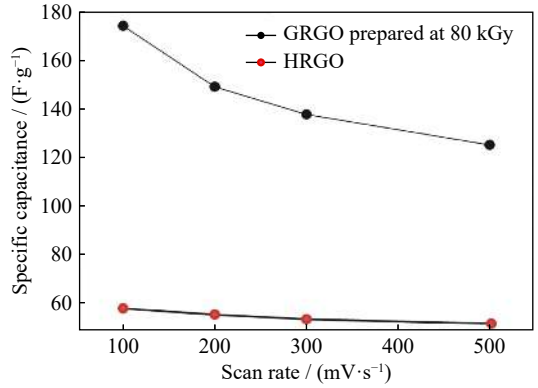

Fig. 12. Specific capacitance versus scan rate plots of HRGO and GRGO prepared at 80 kGy.

The enhanced specific capacitance of GRGO compared with that of HRGO could be explained by the combined effects of increased surface area, residual oxygen functionalities, and a high defective level, as confirmed by the XRD, Raman spectroscopy, and BET specific surface area results [65]. The decrease in specific capacitance of GRGO and HRGO with increasing scan rate could be attributed to the limited ionic penetration of electrolyte ions in the pores of the electrode surface.

4. Conclusion

XRD, FTIR, Raman spectroscopy, and TGA confirmed the removal of most oxygen functional groups and the successful formation of HRGO and GRGOs without deoxygenation. Raman spectroscopy also revealed that irradiation reduction alters the structure of GO and confers it with massive defects, interpreted by the extensive formation of new smaller sp^2-hybridized domains compared with those obtained through chemical reduction. The calculated BET-specific surface area of GRGO prepared at 80 kGy was larger than that of HRGO because irradiation restrains GRGO aggregation. Because of its lower defect level, HRGO showed a higher calculated electrical conductivity compared with the GRGOs. Although defects lowered the electrical conductivity of GRGOs, they also improved the electrochemical performance of the material compared with HRGO. The CV curves of GRGO prepared at 80 kGy exhibited a pseudocapacitive behavior compared with the EDLC performance of HRGO. The maximum specific capacitance of GRGO prepared at 80 kGy was ~174 $F \cdot g^{-1}$, which is higher than that of HRGO (~58 $F \cdot g^{-1}$) at the same scan rate. The enhanced specific capacitance of GRGO prepared at 80 kGy was mainly due to its higher defect level and surface area than HRGO. Moreover, γ-ray reduction showed excellent efficiency for removing thermally-labile oxygen species, thereby enhancing the thermal stability of GRGOs compared with HRGO over a definite temperature range. The above results highlight the potential applications of GRGOs in devices such as supercapacitors and thermos-resistors.

Acknowledgement

This work was financially supported by the International Atomic Energy Agency in the framework of the Coordinated Research Project F22070.

References

[1] K. Le, Z. Wang, F.L. Wang, Q. Wang, Q. Shao, V. Murugadoss, S.D. Wu, W. Liu, J.R. Liu, Q. Gao, and Z.H. Guo, Sandwich-like NiCo layered double hydroxide/reduced graphene oxide nanocomposite cathodes for high energy density asymmetric supercapacitors, *Dalton Trans.*, 48(2019), No. 16, p. 5193.

[2] R. Fang, K. Chen, L. Yin, Z. Sun, F. Li, and H.M. Cheng, The regulating role of carbon nanotubes and graphene in lithium-ion and lithium-sulfur batteries, *Adv. Mater.*, 31(2019), No. 9, art. No. 1800863.

[3] A. Alnuaimi, I. Almansouri, I. Saadat, and A. Nayfeh, High performance graphene-silicon Schottky junction solar cells with HfO_2 interfacial layer grown by atomic layer deposition, *Sol. Energy*, 164(2018), p. 174.
[4] P. Sutter, How silicon leaves the scene, *Nat. Mater.*, 8(2009), No. 3, p. 171.
[5] A. Reina, X.T. Jia, J. Ho, D. Nezich, H. Son, V. Bulovic, M.S. Dresselhaus, and J. Kong, Large area, few-layer graphene films on arbitrary substrates by chemical vapor deposition, *Nano Lett.*, 9(2009), No. 1, p. 30.
[6] Y.B. Zhang, Y.W. Tan, H.L. Stormer, and P. Kim, Experimental observation of the quantum Hall effect and Berry's phase in graphene, *Nature*, 438(2005), No. 7065, p. 201.
[7] M.J. McAllister, J.L. Li, D.H. Adamson, H.C. Schniepp, A.A. Abdala, J. Liu, M. Herrera-Alonso, D.L. Milius, R. Car, R.K. Prud'homme, and I.A. Aksay, Single sheet functionalized graphene by oxidation and thermal expansion of graphite, *Chem. Mater.*, 19(2007), No. 18, p. 4396.
[8] V.B. Mohan, K.T. Lau, D. Hui, and D. Bhattacharyya, Graphene-based materials and their composites: A review on production, applications and product limitations, *Composites Part B*, 142(2018), p. 200.
[9] S. Park, J. An, J.R. Potts, A. Velamakanni, S. Murali, and R.S. Ruoff, Hydrazine-reduction of graphite- and graphene oxide, *Carbon*, 49(2011), No. 9, p. 3019.
[10] D.D. Hou, Q.F. Liu, H.F. Cheng, H. Zhang, and S. Wang, Green reduction of graphene oxide via Lycium barbarum extract, *J. Solid State Chem.*, 246(2017), p. 351.
[11] S. Thakur and N. Karak, Alternative methods and nature-based reagents for the reduction of graphene oxide: A review, *Carbon*, 94(2015), p. 224.
[12] D. Voiry, J. Yang, J. Kupferberg, R. Fullon, C. Lee, H.Y. Jeong, H.S. Shin, and M. Chhowalla, High-quality graphene via microwave reduction of solution-exfoliated graphene oxide, *Science*, 353(2016), No. 6306, p. 1413.
[13] X.R. Zheng, B.H. Jia, X. Chen, and M. Gu, *In situ* third-order non-linear responses during laser reduction of graphene oxide thin films towards on-chip non-linear photonic devices, *Adv. Mater.*, 26(2014), No. 17, p. 2699.
[14] C. Yang, J.Y. Gong, P. Zeng, X.L. Yang, R.Q. Liang, Q.R. Ou, and S.Y. Zhang, Fast room-temperature reduction of graphene oxide by methane/argon plasma for flexible electronics, *Appl. Surf. Sci.*, 452(2018), p. 481.
[15] C.Y. Lin, C.E. Cheng, S. Wang, H.W. Shiu, L.Y. Chang, C.H. Chen, T.W. Lin, C.S. Chang, and F.S.S. Chien, Synchrotron radiation soft X-ray induced reduction in graphene oxide characterized by time-resolved photoelectron spectroscopy, *J. Phys. Chem. C*, 119(2015), No. 23, p. 12910.
[16] B.W. Zhang, L.F. Li, Z.Q. Wang, S.Y. Xie, Y.J. Zhang, Y. Shen, M. Yu, B. Deng, Q. Huang, C.H. Fan, and J.Y. Li, Radiation induced reduction: An effective and clean route to synthesize functionalized graphene, *J. Mater. Chem.*, 22(2012), No. 16, p. 7775.
[17] C.H. Jung, Y.W. Park, I.T. Hwang, Y.J. Go, S.I. Na, K. Shin, J.S. Lee, and J.H. Choi, Eco-friendly and simple radiation-based preparation of graphene and its application to organic solar cells, *J. Phys. D: Appl. Phys.*, 47(2014), No. 1, art. No. 015105.
[18] Y.L. He, J.H. Li, L.F. Li, and J.Y. Li, Gamma-ray irradiation-induced reduction and self-assembly of graphene oxide into three-dimensional graphene aerogel, *Mater. Lett.*, 177(2016), p. 76.
[19] H.T. Zhao, Z.G. Li, N. Zhang, Y.C. Du, S.W. Li, L. Shao, D.Y. Gao, X.J. Han, and P. Xu, γ-irradiation induced one-step synthesis of electromagnetic functionalized reduced graphene oxide–Ni nanocomposites, *RSC Adv.*, 4(2014), No. 57, p. 30467.
[20] M.L. Lu, J.H. Li, L.F. Li, J. Lin, and J.Y. Li, Fabrication of ultralight 3D graphene/Pt aerogel via *in situ* gamma-ray irradiation and its application for the catalytic degradation of methyl orange, *Fullerenes Nanotubes Carbon Nanostruct.*, 28(2020), No. 5, p. 425.
[21] B. Gupta, A.A. Melvin, T. Matthews, S. Dhara, S. Dash, and A.K. Tyagi, Facile gamma radiolytic methodology for TiO_2–rGO synthesis: Effect on photo-catalytic H_2 evolution, *Int. J. Hydrogen Energy*, 40(2015), No. 17, p. 5815.
[22] M.Q. Sun, G.C. Wang, X.W. Li, and C.Z. Li, Irradiation preparation of reduced graphene oxide/carbon nanotube composites for high-performance supercapacitors, *J. Power Sources*, 245(2014), p. 436.
[23] Y.J. Noh, S.C. Park, I.T. Hwang, J.H. Choi, S.S. Kim, C.H. Jung, and S.I. Na, High-performance polymer solar cells with radiation-induced and reduction-controllable reduced graphene oxide as an advanced hole transporting material, *Carbon*, 79(2014), p. 321.
[24] J. Shi, W.W. Jiang, L.S. Liu, M.L. Jing, F.Y. Li, Z.W. Xu, and X.X. Zhang, Elucidating synthesis of noble metal nanoparticles/graphene oxide in free-scavenger γ-irradiation, *Curr. Appl. Phys.*, 19(2019), No. 7, p. 780.
[25] Y.W. Zhang, H.L. Ma, Q.L. Zhang, J. Peng, J.Q. Li, M.L. Zhai, and Z.Z. Yu, Facile synthesis of well-dispersed graphene by γ-ray induced reduction of graphene oxide, *J. Mater. Chem.*, 22(2012), No. 26, p. 13064.
[26] Y. Yang, L. Chen, D.Y. Li, R.B. Yi, J.W. Mo, M.H. Wu, and G. Xu, Controllable reduction of graphene oxide by electron-beam irradiation, *RSC Adv.*, 9(2019), No. 7, p. 3597.
[27] J.M. Jung, C.H. Jung, M.S. Oh, I.T. Hwang, C.H. Jung, K. Shin, J. Hwang, S.H. Park, and J.H. Choi, Rapid, facile, and eco-friendly reduction of graphene oxide by electron beam irradiation in an alcohol–water solution, *Mater. Lett.*, 126(2014), p. 151.
[28] M. Kang, D.H. Lee, J. Yang, Y.M. Kang, and H. Jung, Simultaneous reduction and nitrogen doping of graphite oxide by using electron beam irradiation, *RSC Adv.*, 5(2015), No. 126, p. 104502.
[29] D.C. Marcano, D.V. Kosynkin, J.M. Berlin, A. Sinitskii, Z.Z. Sun, A. Slesarev, L.B. Alemany, W. Lu, and J.M. Tour, Improved synthesis of graphene oxide, *ACS Nano*, 4(2010), No. 8, p. 4806.
[30] A. Buchsteiner, A. Lerf, and J. Pieper, Water dynamics in graphite oxide investigated with neutron scattering, *J. Phys. Chem. B*, 110(2006), No. 45, p. 22328.
[31] V.B. Mohan, R. Brown, K. Jayaraman, and D. Bhattacharyya, Characterisation of reduced graphene oxide: Effects of reduction variables on electrical conductivity, *Mater. Sci. Eng. B*, 193(2015), p. 49.
[32] X.B. Meng, D.S. Geng, J. Liu, M.N. Banis, Y. Zhang, R.Y. Li, and X.L. Sun, Non-aqueous approach to synthesize amorphous/crystalline metal oxide-graphene nanosheet hybrid composites, *J. Phys. Chem. C*, 114(2010), No. 43, p. 18330.
[33] M. Wojtoniszak, X.C. Chen, R.J. Kalenczuk, A. Wajda, J. Łapczuk, M. Kurzewski, M. Drozdzik, P.K. Chu, and E. Borowiak-Palen, Synthesis, dispersion, and cytocompatibility of graphene oxide and reduced graphene oxide, *Colloids Surf. B*, 89(2012), p. 79.
[34] E.Y. Choi, T.H. Han, J. Hong, J.E. Kim, S.H. Lee, H.W. Kim, and S.O. Kim, Noncovalent functionalization of graphene with

end-functional polymers, *J. Mater. Chem.*, 20(2010), No. 10, p. 1907.
[35] A.C. Ferrari, J.C. Meyer, V. Scardaci, C. Casiraghi, M. Lazzeri, F. Mauri, S. Piscanec, D. Jiang, K.S. Novoselov, S. Roth, and A.K. Geim, Raman spectrum of graphene and graphene layers, *Phys. Rev. Lett.*, 97(2006), No. 18, art. No. 187401.
[36] M.J. Allen, V.C. Tung, and R.B. Kaner, Honeycomb carbon: A review of graphene, *Chem. Rev.*, 110(2010), No. 1, p. 132.
[37] K.N. Kudin, B. Ozbas, H.C. Schniepp, R.K. Prud'homme, I.A. Aksay, and R. Car, Raman spectra of graphite oxide and functionalized graphene sheets, *Nano Lett.*, 8(2008), No. 1, p. 36.
[38] F. Tuinstra and J.L. Koenig, Raman spectrum of graphite, *J. Chem. Phys.*, 53(1970), No. 3, p. 1126.
[39] C.T. Hsieh, B.H. Yang, and Y.F. Chen, Dye-sensitized solar cells equipped with graphene-based counter electrodes with different oxidation levels, *Diam. Relat. Mater.*, 27-28(2012), p. 68.
[40] S. Park and R.S. Ruoff, Chemical methods for the production of graphenes, *Nat. Nanotechnol.*, 4(2009), No. 4, p. 217.
[41] S. Stankovich, D.A. Dikin, R.D. Piner, K.A. Kohlhaas, A. Kleinhammes, Y.Y. Jia, Y. Wu, S.T. Nguyen, and R.S. Ruoff, Synthesis of graphene-based nanosheets via chemical reduction of exfoliated graphite oxide, *Carbon*, 45(2007), No. 7, p. 1558.
[42] I.K. Moon, J. Lee, R.S. Ruoff, and H. Lee, Reduced graphene oxide by chemical graphitization, *Nat. Commun.*, 1(2010), art. No. 73.
[43] H.K. Jeong, M.H. Jin, K.P. So, S.C. Lim, and Y.H. Lee, Tailoring the characteristics of graphite oxides by different oxidation times, *J. Phys. D: Appl. Phys.*, 42(2009), No. 6, art. No. 065418.
[44] J.F. Shen, Y.Z. Hu, M. Shi, N. Li, H.W. Ma, and M.X. Ye, One step synthesis of graphene oxide–magnetic nanoparticle composite, *J. Phys. Chem. C*, 114(2010), No. 3, p. 1498.
[45] M. Eizenberg and J.M. Blakely, Carbon monolayer phase condensation on Ni(111), *Surf. Sci.*, 82(1979), No. 1, p. 228.
[46] D.S. Sutar, G. Singh, and V. Divakar Botcha, Electronic structure of graphene oxide and reduced graphene oxide monolayers, *Appl. Phys. Lett.*, 101(2012), No. 10, art. No. 103103.
[47] J.C. Meyer, A.K. Geim, M.I. Katsnelson, K.S. Novoselov, T.J. Booth, and S. Roth, The structure of suspended graphene sheets, *Nature*, 446(2007), No. 7131, p. 60.
[48] G. Eda, G. Fanchini, and M. Chhowalla, Large-area ultrathin films of reduced graphene oxide as a transparent and flexible electronic material, *Nat. Nanotechnol.*, 3(2008), No. 5, p. 270.
[49] C.H. An Wong and M. Pumera, Highly conductive graphene nanoribbons from the reduction of graphene oxide nanoribbons with lithium aluminium hydride, *J. Mater. Chem. C*, 2(2014), No. 5, p. 856.
[50] H.L. Wang, J.T. Robinson, X.L. Li, and H.J. Dai, Solvothermal reduction of chemically exfoliated graphene sheets, *J. Am. Chem. Soc.*, 131(2009), No. 29, p. 9910.
[51] D.C. Wei, Y.Q. Liu, Y. Wang, H.L. Zhang, L.P. Huang, and G. Yu, Synthesis of N-doped graphene by chemical vapor deposition and its electrical properties, *Nano Lett.*, 9(2009), No. 5, p. 1752.
[52] D. Erçin, M. Eken, Z. Aktas, S. Çetinkaya, B. Sakintuna, and Y. Yürüm, Effect of γ-irradiation on the structure of activated carbons produced from Turkish Elbistan lignite, *Radiat. Phys. Chem.*, 73(2005), No. 5, p. 263.
[53] Q.L. Du, M.B. Zheng, L.F. Zhang, Y.W. Wang, J.H. Chen, L.P. Xue, W.J. Dai, G.B. Ji, and J.M. Cao, Preparation of functionalized graphene sheets by a low-temperature thermal exfoliation approach and their electrochemical supercapacitive behaviors, *Electrochim. Acta*, 55(2010), No. 12, p. 3897.
[54] G.P. Xiong, C.Z. Meng, R.G. Reifenberger, P.P. Irazoqui, and T.S. Fisher, A review of graphene-based electrochemical microsupercapacitors, *Electroanalysis*, 26(2014), No. 1, p. 30.
[55] M.Y. Yu, B.Q. Xie, Y. Yang, Y. Zhang, Y. Chen, W.Y. Yu, S.S. Zhang, L.H. Lu, and D. Liu, Residual oxygen groups in nitrogen-doped graphene to enhance the capacitive performance, *RSC Adv.*, 7(2017), No. 25, p. 15293.
[56] D. Hulicova-Jurcakova, M. Seredych, G.Q. Lu, and T.J. Bandosz, Combined effect of nitrogen- and oxygen-containing functional groups of microporous activated carbon on its electrochemical performance in supercapacitors, *Adv. Funct. Mater.*, 19(2009), No. 3, p. 438.
[57] J. Yang and L.D. Zou, Graphene films of controllable thickness as binder-free electrodes for high performance supercapacitors, *Electrochim. Acta*, 130(2014), p. 791.
[58] L. Zhang, X. Yang, F. Zhang, G.K. Long, T.F. Zhang, K. Leng, Y.W. Zhang, Y. Huang, Y.F. Ma, M.T. Zhang, and Y.S. Chen, Controlling the effective surface area and pore size distribution of sp^2 carbon materials and their impact on the capacitance performance of these materials, *J. Am. Chem. Soc.*, 135(2013), No. 15, p. 5921.
[59] Z.Y. Xiong, C.L. Liao, W.H. Han, and X.G. Wang, Mechanically tough large-area hierarchical porous graphene films for high-performance flexible supercapacitor applications, *Adv. Mater.*, 27(2015), No. 30, p. 4469.
[60] J.S. Lee, S.I. Kim, J.C. Yoon, and J.H. Jang, Chemical vapor deposition of mesoporous graphene nanoballs for supercapacitor, *ACS Nano*, 7(2013), No. 7, p. 6047.
[61] G.X. Luo, L.Z. Liu, J.F. Zhang, G.B. Li, B.L. Wang, and J.J. Zhao, Hole defects and nitrogen doping in graphene: Implication for supercapacitor applications, *ACS Appl. Mater. Interfaces*, 5(2013), No. 21, p. 11184.
[62] Z.H. Wen, X.C. Wang, S. Mao, Z. Bo, H. Kim, S.M. Cui, G.H. Lu, X.L. Feng, and J.H. Chen, Crumpled nitrogen-doped graphene nanosheets with ultrahigh pore volume for high-performance supercapacitor, *Adv. Mater.*, 24(2012), No. 41, p. 5610.
[63] G. Moussa, C. Matei Ghimbeu, P.L. Taberna, P. Simon, and C. Vix-Guterl, Relationship between the carbon nano-onions (CNOs) surface chemistry/defects and their capacitance in aqueous and organic electrolytes, *Carbon*, 105(2016), p. 628.
[64] P. Song, X.Y. Zhang, M.X. Sun, X.L. Cui, and Y.H. Lin, Synthesis of graphene nanosheets via oxalic acid-induced chemical reduction of exfoliated graphite oxide, *RSC Adv.*, 2(2012), No. 3, p. 1168.
[65] D. Majumdar, N. Baugh, and S.K. Bhattacharya, Ultrasound assisted formation of reduced graphene oxide-copper (II) oxide nanocomposite for energy storage applications, *Colloids Surf. A*, 512(2017), p. 158.